HHS Public Access

Author manuscript

*Nat Neurosci*. Author manuscript; available in PMC 2018 May 20.

Published in final edited form as:

*Nat Neurosci*. 2018 January ; 21(1): 72–80. doi:10.1038/s41593-017-0022-z.

# Reducing the RNA binding protein TIA1 protects against tau-mediated neurodegeneration *in vivo*

**Daniel J. Apicco**[1], **Peter E. A. Ash**[1], **Brandon Maziuk**[1], **Chelsey LeBlang**[2], **Maria Medalla**[2], **Ali Al Abdullatif**[1], **Antonio Ferragud**[1], **Emily Botelho**[1], **Heather I. Ballance**[1], **Uma Dhawan**[1], **Samantha Boudeau**[1], **Anna Lourdes Cruz**[1], **Daniel Kashy**[1], **Aria Wong**[1], **Lisa R. Goldberg**[1], **Neema Yazdani**[1], **Cheng Zhang**[3], **Choong Y Ung**[3], **Yorghos Tripodis**[4], **Nicholas M. Kanaan**[5], **Tsuneya Ikezu**[1,6], **Pietro Cottone**[1], **John Leszyk**[7], **Hu Li**[3], **Jennifer Luebke**[2], **Camron D. Bryant**[1], and **Benjamin Wolozin**[1,6,*]

[1]Dept. of Pharmacology and Experimental Therapeutics, Boston University School of Medicine, Boston, MA

[2]Dept. of Anatomy, Boston University School of Medicine, Boston, MA

[3]Dept. of Molecular Pharmacology & Experimental Therapeutics, Mayo Clinic, Rochester, MN

[4]Dept. of Environmental Health, Boston University School of Public Health, Boston, MA

[5]Dept. of Translational Science and Molecular Medicine, College of Human Medicine, Michigan State University, East Lansing, MI

[6]Dept. of Neurology, Boston University School of Medicine, Boston, MA

[7]Dept. of Biochemistry and Molecular Pathology, University of Massachusetts Medical Center, Worcester, MA

## SUMMARY

Emerging studies suggest a role for tau in regulating the biology of RNA binding proteins (RBPs). We now show that reducing the RBP T-cell intracellular antigen 1 (TIA1) *in vivo* protects against neurodegeneration and prolongs survival in transgenic P301S tau mice. Biochemical fractionation shows co-enrichment and co-localization of tau oligomers and RBPs in transgenic P301S tau mice. Reducing TIA1 decreases the number and size of granules co-localizing with stress granule markers. Decreasing TIA1 also inhibits the accumulation of tau oligomers at the expense of increasing neurofibrillary tangles (NFTs). Despite the increase in NFTs, TIA1 reduction increases neuronal survival and rescues behavioral deficits and lifespan. These data provide *in vivo* evidence



*Corresponding Author: Benjamin Wolozin, M.D., Ph.D., Professor, Depts. of Pharmacology and Neurology, Graduate Program in Neuroscience, Boston University, School of Medicine, 72 East Concord St., R614, Boston, MA 02118-2526, 617-414-2652 (Phone), bwolozin@bu.edu.

**Conflict of Interest Statement:** Benjamin Wolozin is Co-Founder and Chief Scientific Officer for Aquinnah Pharmaceuticals Inc.

**Author Contributions:**

DJA conceived, performed and analyzed experiments, and wrote the original draft; PEAA performed and analyzed experiments; BM, CL, MM, AAA, EB, HB, DK, AW, LRG, NY and JL (from UMass) performed experiments, AFF, CZ, CYU, NMK, TI, PC, JL (from BU), HL and CB provided expertise and edited the manuscript; BW conceived, analyzed, wrote the original draft, edited, supervised and provided funding for the project.

that TIA1 plays a key role in mediating toxicity, and further suggest that RBPs direct the pathway of tau aggregation and the resulting neurodegeneration. We propose a paradigm in which dysfunction of the translational stress response leads to tau-mediated pathology.

## Keywords

Stress granules; RNA granules; neurodegeneration; tauopathy; transgenic models; neuropathology; behavior; memory; oligomers; protein aggregation

RNA binding proteins (RBPs) are frequently involved in neurodegenerative disease pathology and genetics[1, 2]. RBPs contain low complexity domains that mediate reversible phase transition between soluble and liquid-droplet states. These low complexity domains contain repeat sequences enriched for glycines and uncharged, polar amino acids, and are intrinsically disordered[3, 4]. Self-assembly of these low complexity domains promotes regulated aggregation of RBPs and client mRNA transcripts to form RNA granules, which control RNA metabolism[5]. Cytoplasmic RNA granules are abundant in neurons because of the extensive transport and local regulation of mRNAs required at synapses. RNA granules also mediate the translational response to stress, forming stress granules (SGs) which function, in part, to transiently sequester transcripts that are unnecessary for the stress response[6]. SGs are classically defined by cytoplasmic co-localization of particular RBPs in the context of a stress (including TIA1 and Poly(A) binding protein, PABP)[5]. Because the nature of SGs in chronic diseases have not been well characterized, we will use the term “pathological SG” (pSG) to reflect a potential distinction between RBP granules containing TIA1 that occur in cell culture and those that occur *in vivo*.

Aggregation mediated by low complexity domains in RBPs appears to be critical for the involvement of RBPs in disease. Mutations in RBPs cause Amyotrophic Lateral Sclerosis (ALS), Frontotemporal dementia (FTD), Spinocerebellar Ataxia and myopathies[2]. Some of these disease-linked RBPs also form pathological aggregates in these diseases (i.e. TDP-43, FUS, TIA1)[7]; in spinocerbellar ataxias poly-glutamine repeats tend to aggregate, but the trinucleotide repeats also appear to form liquid droplets[8]. Many disease-linked mutations in RBPs, such as in FUS and hnRNPA1, accelerate phase transitions of recombinant RBPs from soluble to liquid-droplet states, which promotes the irreversible transition from liquid-droplet to insoluble fibrils inducing amyloids that are putatively pathological[9–12]. Thus, dysfunction of RBPs appears to greatly influence the development of neurodegenerative disease.

Recent results suggest that aggregation of RBPs is also a pathological feature in tauopathies[13, 14]. Various RBPs, including the SG nucleating protein TIA1, co-localize with hyper-phosphorylated tau in patient tissues and progressively accumulate with aggregated tau in mouse models of disease (Tg4510, JNPL3 and PS19)[13, 14]. However, whether SGs or RBPs contribute to the progression of tauopathies is unknown.

The aggregation of tau is a defining pathological hallmark of tauopathies such as Alzheimer’s disease (AD) and FTD-tau. Tau is normally located in axons where it functions to bind and stabilize microtubules, but in tauopathies, pathological tau accumulates in the

somatodendritic compartment, where it form oligomers and fibrils[15]. Our lab recently demonstrated in cell culture that pathological tau promotes the aggregation of RBPs, including TIA1, to form SGs, and that preventing SG formation through reductions in TIA1 levels led to a decrease in tau pathological markers *in vitro*[14]. These results raise the possibility that SGs play an important role in tau-mediated neurodegeneration. Here, we show that reducing TIA1 *in vivo* decreases pSGs, protects against neurodegeneration, improves memory and prolongs the lifespan in PS19 transgenic tau mice. Surprisingly, this behavioral protection occurs despite the increased accumulation of neurofibrillary tangles (NFTs). Strikingly, we show that levels of TIA1 control the accumulation of tau oligomers and associated RBPs. This work suggests that the pathophysiology of tauopathy is dependent on the interaction of tau with RBPs, and add tauopathies such as AD and FTD to the growing list of diseases linked to the dysfunction of RNA metabolism.

## RESULTS

### *Tia1* haploinsufficiency reduces cytoplasmic translocation of Tia1 and SG formation

The PS19 transgenic mouse line, which overexpresses human P301S 1N4R tau under the control of the mouse prion promoter, was utilized to investigate whether reduction in endogenous TIA1 also protects against the progression of tauopathy *in vivo*[16]. We bred PS19 mice with *Tia1*−/− mice to generate littermate tauopathy mice that possess either 1 or 2 copies of the *Tia1* allele, which we will refer to as P301S *Tia1+/−* and P301S *Tia1+/+* mice, respectively[17]. Analysis of endogenous TIA1 protein levels in the brain by immunoblot confirmed that TIA1 protein expression was reduced by >50% in 3-month old P301S *Tia1+/−* compared to P301S *Tia1+/+* mice (Fig. 1A–B).

We next investigated whether P301S *Tia1+/−* mice exhibited reduced cytoplasmic TIA1 granules. Immunohistochemistry (IHC) of hippocampal neurons in P301S *Tia1+/−* mice revealed a greater than 50% reduction in the number of cytoplasmic TIA1 granules compared to P301S *Tia1+/+* mice (Supplemental Fig. S1A–B, hippocampus of 6-month old mice shown), as well as a similar reduction in cytoplasmic TIA1 puncta co-localizing with the SG marker PABP (Fig. 1C–D, lateral entorhinal cortex of 9-month old mice shown). The P301S *Tia1+/+* mice also exhibited considerable depletion of nuclear TIA1, consistent with the disease process producing chronic stress (Fig. 1). In contrast, P301S *Tia1+/−* mice were protected against loss of nuclear TIA1 (Fig. 1E–F). IHC for markers of other types of RNA granules demonstrated that TIA1 reduction increased immunofluorescence levels and puncta for the transport granule marker Staufen and the Processing body (P-body) marker DCP1A (Fig. 1G–K). These data show that heterozygous knockout of *Tia1* selectively inhibits the formation of cytoplasmic TIA1 granules and loss of nuclear TIA1 *in vivo*.

### TIA1 reduction protects against synaptic and neuronal loss in PS19 mice

We proceeded to investigate whether TIA1 reduction also reduces synaptic and neuronal degeneration *in vivo*. PS19 mice exhibit progressive neuronal loss between 6 and 12 months of age that is preceded by presynaptic degeneration[16]. We examined the CA3 region of the hippocampus due to the high density of axon terminals and neuronal cell bodies, and because synaptic and neuronal loss in PS19 mice are well characterized in this region.

Compared to non-transgenic littermates, 6-month old P301S *Tia1+/+* mice exhibited reduced immunofluorescence of synaptophysin (SYP), a presynaptic terminal protein, consistent with prior reports (Fig. 2A–B)[16]. In contrast, SYP immunofluorescence was rescued in P301S *Tia1+/−* compared to P301S *Tia1+/+* mice (Fig. 2A–B), indicating reduced presynaptic degeneration. We also immunostained P301S *Tia1+/+* and P301S *Tia1+/−* for a second axonal structural protein, neurofilament (NFL) (Supplemental Fig. S2). While P301S *Tia1+/+* mice exhibited decreased immunofluorescence of NFL in 9-month CA3, TIA1 haploinsufficiency increased NFL immunofluorescence to a level comparable to non-transgenic controls (Supplemental Fig. S2A–C). Thus, TIA1 reduction appears to protect against presynaptic degeneration up to 9 months of age in P301S tau mice.

Tau binds and stabilizes microtubules (MTs), which promotes axonal outgrowth and fast axonal transport. We investigated whether TIA1 reduction might protect binding of tau to MTs in these mice. MT-bound (pellet, P) and unbound (supernatant, S) fractions were separated by centrifugation in RAB buffer, as described previously[16]. As expected, tau progressively accumulated in the MT-unbound (S) fraction of P301S *Tia1+/+* mice between 6 and 9 months of age, indicating dissociation of tau from MTs (Fig. 2C). In contrast, significantly less tau was detected in the MT-unbound (S) fraction of P301S *Tia1+/−* mice, resulting in a 3-fold increase in the ratio of MT-bound (P) to unbound (S) tau at 9 months of age (Fig. 2C–D, Supplemental Fig. S3). These data indicate that TIA1 reduction protects the synaptic arbor against tau-mediated degeneration while providing an associated stabilization of MTs.

We proceeded to quantify total neuron numbers in the hippocampus (CA3) and lateral entorhinal cortex (LEnt) of P301S *Tia1+/+* and P301S *Tia1+/−* mice. As previously reported, neurons in the hippocampus of P301S TIA+/+ mice were reduced by 6 months[16]. The number of Nissl-positive neurons and NeuN (neuron specific nuclear protein)-positive nuclei were increased in P301S *Tia1+/−* mice compared to P301S *Tia1+/+* mice in both CA3 and LEnt at 9 months of age (Fig. 3A–C, Supplemental S4A). We also assessed the effect of TIA1 reduction on gross cortical atrophy by measuring the distance between the most superficial part of Layer II (Fig. 3D, red asterisks) and the deepest part of Layer III (Fig. 3D, red arrowheads) in the LEnt and primary somatosensory cortex of 9-month P301S *Tia1+/+* and P301S *Tia1+/−* mice. P301S *Tia1+/+* mice exhibited a 54 and 21 percent reduction in Layer II/III thickness in LEnt and primary somatosensory cortex, respectively, while P301S *Tia1+/−* mice were not significantly different from non-transgenic mice (Fig. 3E, Supplemental S4B). Taken together, our data suggests that TIA1 reduction protects against tau-mediated neurodegeneration *in vivo*.

## TIA1 reduction alleviates cognitive impairment and extends lifespan in PS19 mice

We next sought to determine whether TIA1 reduction improved the behavioral phenotype of PS19 mice. Previous studies found that PS19 mice exhibit cognitive impairment[18]. In the Y maze spontaneous alternation task (SAT), 6-month P301S *Tia1+/+* mice exhibited reduced spontaneous alternation compared to non-transgenic mice (Fig. 4A), indicating an impairment in spatial working memory similar to that previously reported in PS19 mice. Remarkably, P301S *Tia1+/−* mice rescued the behavioral deficit to normal working memory

levels (Fig. 4A); TIA1 reduction had no effect in non-transgenic mice (Fig. 4A). We also employed a second behavioral task, the novel object recognition (NOR) task, to assess recognition memory and independently confirm the beneficial effect of TIA1 reduction in a separate domain of cognitive function. As expected, 6-month P301S *Tia1+/+* mice were not able to distinguish between the novel and familiar objects, indicating an impairment in recognition memory (Fig. 4B). In contrast, P301S *Tia1+/−* mice exhibited greater than 65% preference indices for the novel object, confirming a restoration of functional recognition memory to levels similar to that seen in non-transgenic animals (WT Tau *Tia1+/+* and WT Tau *Tia1+/−*) (Fig. 4B). Importantly, P301S *Tia1+/+* and P301S *Tia1+/−* mice did not differ in the amount of locomotor activity in the SAT or OF tasks, indicating that their improved memory performance could not be attributed to differences in locomotor or anxiety-like behaviors (Fig. 4C, Supplemental Fig. S5, S6A–D). While both SAT and NOR tasks depend in part on hippocampal function, the SAT depends on additional circuitry, including the prefrontal cortex, basal forebrain, and dorsal striatum[19] whereas the NOR more selectively depends on the hippocampus and perirhinal cortex[20]. The improvement in behavior obtained from these two distinct memory tasks suggests that TIA1 reduction might confer widespread protection against neurodegeneration. These results suggest that RBPs exert an especially important influence on tau-mediated perturbations related to cognition, which is the primary clinical feature of tauopathies.

As our data also suggests that TIA1 reduction protects against tau-mediated neurodegeneration *in vivo* (Fig. 3), we sought to determine whether TIA1 reduction could increase the lifespan of PS19 mice. A previous study found that PS19 mice die prematurely due to motor ataxia and hindlimb paralysis, with a reported median survival of 9 months and 80% mortality by 12 months of age[16]. Our cohort of P301S *Tia1+/+* mice recapitulated this lifespan phenotype (Fig. 4D). In contrast, the P301S *Tia1+/−* mice exhibited a striking increase in lifespan (mean lifespan = 11.3 months, n = 23; compared to 9.3 months for P301S *Tia1+/+*, n=20), with 43.5% surviving to 12 months of age without exhibiting overt symptoms of disease (e.g., ataxia, hind limb weakness, hunched posture, etc.) (Fig. 4D, Supplemental Table S1). Further, 5 of 21 (23.8%) P301S *Tia1+/−* mice that were allowed to age until 15 months survived compared to none (0.0%) of the P301S *Tia1+/+* mice (Fig. 4D, Supplemental Table S1). As expected, all of the non-transgenic mice in this study (WT Tau *Tia1+/+*, n=12; WT Tau *Tia1+/−*, n=16) survived to 12 months of age without evidence of motor or neurological symptoms (not shown). Thus, TIA1 reduction extends median lifespan by 21.5% in PS19 mice. These findings indicate that TIA1 reduction confers robust behavioral protection against tau-mediated neurodegeneration and premature mortality in PS19 mice.

### TIA1 reduction initially decreases tau phosphorylation

Tau is hyper-phosphorylated in AD and FTD-tau, with hyper-phosphorylation leading to tau aggregation and subsequent pathology. We compared the age-dependent accumulation of phosphorylated tau in P301S *Tia1+/+* and P301S *Tia1+/−* mice by IHC. As expected, P301S *Tia1+/+* mice accumulated detectable levels of CP13 (S202)- and AT8 (S202/T205)-phosphorylated tau in the hippocampus by 3 months of age (Supplemental Fig. S7). Little to no phosphorylated tau was observed in the cortex or cerebellum of P301S *Tia1+/+* mice at 3

months of age, consistent with the expected progression of disease in PS19 mice (not shown). In contrast, P301S *Tia1+/−* mice exhibited reduced levels of CP13- and AT8-phosphorylated tau in the hippocampus (CA1, CA3) compared to P301S *Tia1+/+* mice at 3 months of age (Supplemental Fig. S7B-C), suggesting that TIA1 reduction delays the onset of pathology in PS19 mice. This reduction of tau pathology in young P301S *Tia1+/−* mice is consistent with our prior short-term studies using cultured neurons[13].

We proceeded to determine how TIA1 reduction affected tau phosphorylation at later stages of disease by measuring the levels of AT8-, CP13-, and PHF1-phosphorylated tau at 6 and 9 months of age. Surprisingly, TIA1 reduction led to increased immunofluorescence for AT8- and CP13-phosphorylated tau at 6 and 9 months (Supplemental Fig. S7D, CP13 data shown). TIA1 reduction also increased the number of PHF1-positive inclusions in LEnt and CA3 at 9 months of age (Fig. 5A–B). While almost 20% of PHF1-positive inclusions co-localized with cytoplasmic TIA1 in P301S *Tia1+/+* mice, less than 5% of PHF1 inclusions contained TIA1 in P301S *Tia1+/−* mice (Fig. 5C–D). The P301S *Tia1+/−* mice also showed a striking rescue of TIA1 nuclear localization, with TIA1 being largely restricted to the nucleus even in PHF1-positive neurons (Fig. 5C). Immunoblot analysis of total brain lysates confirmed that levels of CP13- and PHF1-phosphorylated tau were increased in aged P301S *Tia1+/−* compared to P301S *Tia1+/+* mice (Supplemental Fig. S8A–C); total tau levels were also slightly elevated (Supplemental Fig. S8D). Thus, TIA1 reduction initially decreased the level of phosphorylated tau pathology in PS19 mice, but then exhibited an age-dependent increase in phosphorylated tau at later stages of disease.

## TIA1 reduction accelerates neurofibrillary tangle accumulation while decreasing levels of soluble tau oligomers

Tau phosphorylation leads to aggregation of tau proteins[21, 22]. Consistent with the age-dependent increases in tau phosphorylation, an increase in neurofibrillary tangles (NFTs) was also apparent in P301S *Tia1+/−* mice. As expected, 9-month P301S *Tia1+/+* mice developed widespread Gallyas silver- and thioflavine S (ThioS)-positive tangles throughout the hippocampus and temporal cortex (Fig. 5E–H). P301S *Tia1+/−* mice exhibited increased numbers of Gallyas silver-positive neurons in both the frontal (primary motor area, M1) and temporal (LEnt) cortices (Fig. 5F); TIA1 reduction also increased the level of ThioS fluorescence (Fig. 5G–H). The number of Gallyas silver-positive tangles did not differ between P301S *Tia1+/+* and P301S *Tia1+/−* mice in the CA3 region of the hippocampus, perhaps resulting from a “ceiling effect” caused by the advanced level of pathology in CA3 relative to other brain areas in this model (Fig. 5F). Despite equal number of NFTs in CA3 at 9 months of age, there was no relationship between tangle burden and neuronal loss in either P301S *Tia1+/+* or P301S *Tia1+/−* mice ($r^2 = 0.07$; Supplemental Fig. S9). Thus, the neuroprotection associated with TIA1 reduction in PS19 mice occurred independently from NFTs, consistent with previous studies suggesting that NFTs are not the direct cause of neuronal loss in tauopathies[23–25].

The improved functional phenotype in P301S *Tia1+/−* mice despite increased tau pathology led us to hypothesize that TIA1 reduction alters the structural or biochemical properties of tau aggregates, producing tau species that are less toxic. This possibility seemed particularly

plausible given the recent findings that neurons containing NFT-like inclusions remain functional and that different strains of tau aggregates exhibit distinct patterns of propagation and pathophysiology when injected into tauopathy mice[23–27]. Biochemical fractionation studies identify tau species with distinct structural properties that are apparent upon separation of TBS-extractable (S1), sarkosyl-soluble (S3), and sarkosyl-insoluble (P3) fractions[28]. A second high-speed spin of the S1 fraction yields a supernatant (S1c) and insoluble pellet (S1p) fraction. The insoluble material (S1p) from the TBS-extractable fraction contains oligomeric tau species that correlate with neurodegeneration in rTg4510 mice, while the P3 fraction contains mostly fibrillar, hyper-phosphorylated (CP13-/PHF1-positive) tau[29]. Similar approaches using 6- and 9-month P301S *Tia1+/+* and P301S *Tia1+/−* mice showed that tau progressively accumulates in both the S1p and P3 fractions of P301S *Tia1+/+* mice (Fig. 6A–C), suggesting accumulation of both oligomeric tau and NFTs, respectively. In the S1p fraction, immunoblotting for total tau identified predominant bands under non-reducing conditions at 64, 140 and 170 kD, confirming the presence of both tau monomers and oligomers in this fraction (Fig. 6A). Surprisingly, while TIA1 reduction increased NFTs (Fig. 5) and showed a concomitant increase in the level of tau in the P3 fraction, TIA1 reduction greatly decreased the level of all tau isoforms detected in the S1p fraction (Fig. 6A–B). ELISAs performed using non-denaturing conditions with antibodies that recognize pathological conformations of misfolded (TNT1, recognizing exposure of the phosphatase-activating domain [PAD]) and oligomeric (TOC1) tau showed reduced levels of misfolded and oligomeric tau in the S1 fraction (Supplemental Fig. S10)[30]. This result suggests that TIA1 reduction shifts the pathway of tau aggregation preventing the accumulation of oligomeric tau while promoting the accumulation of fibrillar tau.

## TIA1 drives the accumulation of tau oligomers

Since aggregation of tau oligomers in the S1p fraction was sensitive to TIA1 reduction, we next investigated whether other RBPs co-aggregated with tau oligomers. We analyzed the S1p (‘tau oligomer’) cortical fraction by OrbiTrap liquid chromatography tandem mass spectrometry (LC-MS/MS) in order to determine if this biochemical fraction is enriched for other RBPs. As expected, the level of tau protein detected in the S1p fraction was significantly elevated in P301S *Tia1+/+* compared to non-transgenic (WT Tau *Tia1+/+*) cortex (Supplemental Table 2). We then used the Database for Annotation, Visualization, and Integrated Discovery (DAVID)[31] to analyze the proteins identified in the S1p fraction of P301S *Tia1+/+* cortex by LC-MS/MS. These studies revealed statistically significant enrichment (False Discovery Ratio, FDR<0.05) for annotations related to RNA metabolism (Supplemental Fig. S11A). In comparison to WT mice, Poly(A) RNA binding was the most significant gene ontology (GO) annotation term enriched among proteins that accumulate in the S1p fraction of P301S *Tia1+/+* compared to non-transgenic mice (Supplemental Fig. S11A and Supplemental Table 2; FDR=2.25E-5). Immunoblot analysis confirmed an age-dependent accumulation of RBPs in both the S1p and P3 fractions of P301S *Tia1+/+* mice (Supplemental Fig. S11B). TIA1 reduction selectively decreased the level of the RBPs PABP and DDX6 in the S1p, but not the P3, fraction (Supplemental Fig. S11B). Taken together, these results suggest that RBPs co-accumulate with tau oligomers in a manner dependent on TIA1.

We proceeded to examine whether TIA1 directly influences tau aggregation. Fibrillization of tau and phospho-tau was studied by thioflavine T (ThioT) fluorescence; phosphorylated 0N4R tau was prepared by reaction with glycogen synthase kinase 3-β (GSK3β) for 30 min, and validated by immunoblot with PHF1 antibody. Fibrillization of tau was examined by incubating 10 μM tau or GSK3β-phosphorylated tau (pTau) ± 2 μM TIA1, total RNA (20 ng/μl), and dextran sulfate (0.04 μg/μl) in the aggregation reaction mixture. Tau fibrillization was significantly reduced in the presence of TIA1 (Fig. 7A). TIA1 also produced significantly more tau oligomers, as quantified by ELISA using the TOC1 anti-oligomeric tau antibody (Fig. 7B). Analysis of the aggregation mixtures by electron microscopy (EM) showed that the presence of TIA1 significantly disrupted fibrillization of tau, producing significantly shorter fibril lengths than similar mixtures incubated without TIA1 (Fig. 7C–D, Supplemental Fig. 12). We proceeded to double immuno-gold label the 48 h pTau assembly reactions with antibodies to TIA1 and either Tau13 (to visualize all tau aggregates, including fibrils) or TOC1 (to visualize pre-fibrillar tau oligomers). Analysis by EM confirmed the presence of both Tau13-positive tau fibrils and TOC1-positive tau oligomers (Supplemental Fig. S13). No TOC1 or TIA1 immunostaining was observed on long fibrillar tau aggregates (Supplemental Fig. S13). In contrast, TIA1 co-labeled pre-fibrillar tau aggregates also positive for TOC1 (Supplemental Fig. S13), suggesting a selective association of TIA1 with tau oligomers. The specificity of TOC1 was validated by the absence of labeling of cortical tissues from WT mice, which contrasted with robust reactivity in P301S tau mice (Supplemental Fig. S14).

## DISCUSSION

Dysfunction of RBPs is implicated in multiple neurodegenerative diseases[32, 33]. Our results now show that TIA1 and other RBPs accumulate in concert with oligomeric tau in an animal model of tauopathy. Importantly, reducing TIA1 leads to the selective reduction of tau oligomers, with a corresponding increase in sarkosyl-insoluble tau fibrils. This reduction in oligomeric tau occurs in parallel with strong neuroprotection, behavioral rescue and increased longevity in the P301S *Tia1+/−* mice, demonstrating an important role for TIA1 in directing the pathway of tau aggregation and the resulting neurodegeneration.

The classic model for protein aggregation in neurodegenerative diseases posits that proteins with disordered or hydrophobic regions inappropriately aggregate through a process of random association that has little or no biological function[34]. This model might well reflect the mechanism driving the aggregation of amyloids that accumulate in the extracellular compartment, such as β-amyloid. However, recent discoveries support an alternative model reflecting the biological functions of RBPs and many nuclear proteins. These proteins all contain low complexity domains whose biophysical properties promote aggregation under normal physiological conditions[9–12, 35]. At high concentrations, recombinant RBPs self-aggregate, forming liquid-like droplets that phase separate, and are able to cycle between liquid and solid states in response to temperature[9–12]. This process leads to formation of membrane-less organelles, including SGs, transport granules and P-bodies, and nuclear structures, such as the nucleolus and PML bodies[4, 36–38].

We recently demonstrated that tau acts as part of the translational stress response to promote formation of SGs, which allows the neuron to adapt its pattern of protein synthesis to cope with stress[13]. Internalization of extracellular tau, such as might occur with propagation, also appears capable of inducing SGs[39]. Somatodendritic mislocalization would allow tau to interact with RBPs, RNA, and ribosomes, which provides a mechanism through which tau can inhibit protein synthesis[40]. Potential mechanistic underpinnings for the interaction of tau with SGs was recently provided by the discovery that tau undergoes liquid-liquid phase separation in the presence of RNA[41]. Thus the abundance of RNA in SGs (and potentially other RNA granules) might be sufficient to stimulate oligomerization and/or liquid-liquid phase separation of tau. This combined work presents a biological explanation for why neurons would have tau mislocalize to the somatodendritic arbor and aggregate during stress. We also observed that the association of tau with SGs promotes its aggregation[13]. These accumulating observations raise the possibility that SGs and perhaps other RNA granules contribute to the pathophysiology of tauopathy.

Because SGs have not been well characterized *in vivo* in the context of disease, we refer to the *in vivo* equivalent as pathological stress granules (pSGs). The dynamics and full composition of the pSGs observed in the P301S mice remains to be determined, which means that the nature of pSGs could differ from classic SGs. Co-localization of tau with the SGs is a parsimonious definition of a pSG that would be prominent in tauopathy. In addition, both pSGs and tau pathology might evolve with time, raising the possibility that the composition might differ based on disease stage.

The current study directly addresses the process of tauopathy in the aging brain *in vivo*. We discovered that the relative accumulation of tau oligomers and fibrils can be regulated by TIA1, suggesting a more general role for RBPs in this process. The process of tau aggregation is known to proceed through multiple steps, including misfolding, oligomerization and fibrillization, but how RBPs might interact with these intermediates is unknown[42]. Using electron microscopy, we demonstrate the surprising finding that TIA1 stabilizes pre-fibrillar tau aggregates, and inhibits their further assembly into large fibrils. We also used mass spectrometry to analyze the oligomeric fraction from diseased brains, and observed a striking enrichment of RBPs in P301S *Tia1+/+* compared to wildtype or P301S *Tia1+/−* samples. This demonstrates that the association of tau with RBPs is likely not limited to TIA1, which is consistent with our prior network analysis showing multiple proteins whose association with TIA1 was dependent on tau[13]. These results now allow us to extend the model of tau aggregation to propose that tau oligomers selectively associate with RBPs, raising the possibility that tau oligomers might be an active species in promoting pSGs and the translational stress response. The putative importance of tau oligomers in the interactions with TIA1 and RNA is supported by a recent study demonstrating that tau phase separates in the presence of RNA[41]. The concentrations of RNA that we use are significantly lower, but the presence of TIA1 in our mixtures might allow for local concentration of RNA much like what might be predicted to occur in a SG.

Neurodegenerative diseases related to aging arise only after an extended period of time and evolve at a slower pace than *in vitro* studies, which highlights the inherent challenge of translating findings from simplified models with recombinant proteins or cultured cells to

mouse models and human patients. We show that reducing TIA1 in PS19 mice elicits a striking reduction in an otherwise over-abundant pSG response. Importantly, reducing TIA1 also correlates with an increase in neuronal survival, improvements in memory and an extension of lifespan. The striking reduction in tau oligomers and corresponding increase in tau fibrils associated with TIA1 haploinsufficiency suggest that the RBPs associated with pSGs (including TIA1) stabilize tau oligomers leading to their accumulation and subsequent pathological responses (Supplemental Fig. 15). In absence of the pSG response, the over-expressed tau in these brains accumulates as tau fibrils, through a process that likely transits rapidly through the oligomer stage or proceeds through an alternative mechanism. AD and other tauopathies do not arise from overexpression of tau, suggesting that tau aggregation in humans might be driven by mass action less compared to animal models. The absence of a pSG response also correlates with behavioral improvements in the PS19 mice, suggesting a scenario in which the association of tau with pSGs might exert a larger role on neurodegeneration in humans, increasing the potential for therapeutic utility.

RBPs such as TIA1 have multiple roles in the cell, regulating RNA localization and utilization in the soma and dendritic arbor, and processes such as splicing and RNA polymerase procession in the nucleus[43, 44]. The pleiotropic roles of TIA1 raises the possibility the TIA1 reduction protects against tauopathy through multiple mechanisms. A full mechanistic understanding will likely be elucidated as research on this pathway progresses.

This work presents tauopathy in a new light, placing it on the spectrum of diseases associated with RBPs. FTD is thought to exist as a continuum with ALS. Many of the genes that cause ALS also cause or appear as pathological species in FTD[37]. We recently demonstrated that somatodendritic tau regulates RBP biology in cultured neurons, suggesting that tau is a functional member of this cohort of proteins[13]. The current work demonstrates that RBPs regulate the pathophysiology of tau, suggesting a novel paradigm for the genesis of tauopathy. Our results provide a model that begins to link the rapid biophysics of liquid-liquid phase separation with the course of neurodegenerative disease, which can take months to years. This evolving model provides a mechanistic site for entry of RBPs into the process of tau aggregation and subsequent tau-mediated neurodegeneration, which opens up many additional targets for therapeutic investigation in the treatment of AD and other tauopathies.

## MATERIALS AND METHODS

### Animals

*Tia1*−/− mice (B6.129S2(C)-Tia1$^{tm1Andp}$/J) were generated by Anderson and colleagues and obtained from Harvard University, Dana Farber Cancer Institute[17]; these mice had previously been backcrossed for 10+ generations to the C57BL/6J inbred strain. PS19 (B6;C3-Tg(Prnp-MAPT*P301S)PS19Vle/J, stock #008169) and C57BL/6J (stock #000664) mice were purchased from Jackson Laboratory[16]. All animals were housed in IACUC-approved vivariums at Boston University School of Medicine. To generate colonies of P301S *Tia1+/+* and P301S *Tia1+/−* mice, PS19 mice were bred with *Tia1*−/− mice to produce pups that were heterozygous for the endogenous mouse *Tia1* allele (*Tia1+/−*) and

either transgenic (P301S+/−, or 'P301S Tau') or non-transgenic (P301S−/−, or 'WT Tau') for human P301S *Mapt*. Transgenic (P301S+/− *Tia1+/−*) and non-transgenic (P301S−/− *Tia1+/−*) pups from the F1 generation were then bred to produce littermate control P301S *Tia1+/+* and P301S *Tia1+/−* mice on identical genetic backgrounds, which were then used in the experiments described in this manuscript. This breeding scheme generated the expected Mendelian ratios of offspring (25% *Tia1+/+*, 50% *Tia1+/−*, and 25% TIA1−/−); however, prior to extensive backcrossing, early generations of pups produced fewer mice than expected with the TIA1−/− genotype. Thus, analysis of P301S TIA1−/− mice was excluded from this study due to insufficient sample sizes. Unless noted otherwise, equal numbers of male and female mice were used in all experimental comparisons; no statistically significant differences with respect to sex were observed in any of the experiments described in this study (data not shown). Due to the necessity to genotype the mice, randomization was not possible for group selection. However, whenever possible, experimenters were blinded to the genotype of each mouse, which was then decoded using the ear-tag identification numbers after data collection and analysis. Mice were aged to 3, 6, and 9 months for analysis by the behavioral, biochemical, and histological approaches described below. Sample sizes were chosen based on prior publications using these mice[16]. The animal care and use committee for Boston University Medical Center approved the animal protocols used in this manuscript.

## Genotyping

Tail snips from ear tagged mice were digested using Proteinase K, and the DNA was purified using the Qiagen DNeasy kit according to manufacturer's instructions (cat# 69504). The human 1N4R P301S transgene was amplified using the following primers (hTau Forward = GGG GAC ACG TCT CCA CGG CAT CTC AGC AAT GTC TCC; hTau Reverse = TCC CCC AGC CTA GAC CAC GAG AAT), using the cycling parameters specified by The Jackson Laboratory (https://www2.jax.org/protocolsdb/f?p=116:5:0::NO:5:P5MASTER_PROTOCOL_ID,P5_JRS_CODE:25393,008169). Mice were also genotyped for both the wildtype *Tia1* allele (WT mTia1 Forward = CTC CTT TAC CAG GAC CAC CA; WT mTia1 Reverse = ACC ATG GGG AAA AGG AGG TA) and frame shifted mutant allele that does not encode TIA1 protein (Mutant mTia1 Forward = CTC CTT TAC CAG GAC CAC CA; Mutant mTia1 Reverse = GCC AGA GGC CAC TTG TGT AG), also using the cycling parameters specified by The Jackson Laboratory (https://www2.jax.org/protocolsdb/f?p=116:5:0::NO:5:P5_MASTER_PROTOCOL_ID,P5_JRS_CODE:23469,009248). Amplified DNA was separated by electrophoresis in a 2% agarose gel, and visualized with 1% ethidium bromide using a BioRad imager.

## Behavioral analysis

All behavioral analyses utilized equal numbers of male and female mice, and were performed at 6 months of age prior to the onset of the neuromuscular symptoms of disease (i.e. ataxia, hind limb weakness/paralysis). For the Open Field (OF) assay, mice were placed in a light- and sound-proof chamber (22 cm wide x 42 cm long) and recorded for 30 min using infrared cameras (Swann Security, Victoria, Australia). Total locomotor activity, center time, mean speed, and freezing behaviors, amongst other parameters, were automatically measured using ANY-maze behavioral tracking software (Stoelting, Wood Dale, IL). For the

Y maze spontaneous alternation task (SAT), animals were placed in an opaque, Y shaped maze with 3 arms of equal length (15 inches each) that diverged at equal angles, and recorded for 10 min. The total number and sequence of arm entries over the test period was scored by 2 blinded observers. A successful alternation was defined as consecutive entries into all three arms without returning to a previously visited arm. Thus, the maximum number of alternations was the total number of arm entries minus two, and the correct alternation percentage was calculated as (actual alternations/maximum alternations)×100. For the novel object recognition (NOR) test, animals were habituated to the testing chambers for 30 min for 2 consecutive days prior to testing day. The testing chambers were rectangular (22 cm wide x 42 cm long) apparatuses completely covered on the outside in 4 different patterns of construction paper to make the environment opaque and to allow the mice to spatially orient themselves in the apparatus. The 4 patterns used for the wall cues were blank (white), polka dots, horizontal bars, and vertical bars (all black and white). On testing day, animals were placed in the chamber and allowed to explore 2 identical objects for 5 min (exploration phase). 90 min later, the animals were returned to the testing chamber with one of the two objects replaced with a novel object. The exploratory behavior of the animals was recorded for 5 min using infrared cameras (Swann Security, Victoria, Australia). The objects used in the study were T-25 cell culture flasks filled with sand and multi-colored rectangular lego stacks, as described previously[45]. All experimental factors, including the type and location of the novel object, were counterbalanced throughout the experiment. Mice that did not explore the objects for at least 10 s during the exploration phase were excluded from analysis in the testing phase. The amount of time spent exploring the familiar and novel objects, determined by head placement within 0.5 cm of each object, was automatically measured using ANY-maze behavioral tracking software (Stoelting). For the survival study, animals were assessed daily starting at 7 months of age by the veterinary staff of the Boston University Animal Science Center, who were blinded to the genotype of the animals. The endpoint criterion was defined as at least one of the following: dragging or paralysis of 2 or more limbs, postural instability/inability to feed, or greater than 10% loss in body weight.

## Tissue Processing

Animals were deeply anesthetized and perfused with ice cold phosphate buffered saline (PBS), followed by brain dissection. The left hemisphere was fixed in 4% paraformaldehyde/PBS for 24 h, and then transferred to 30% sucrose/PBS solution for 48 h prior to freezing in OCT media for cryo-sectioning. We used a fixation time of 24 h because prior optimization experiments for TIA1 (and other RBP) immunohistochemistry demonstrated that fixation for longer periods reduces the ability to detect inclusions containing TIA1. Brains were cut into 40 μm coronal sections and stored at −20°C in 30% glycerol/30% ethylene glycol/PBS solution until day of staining. From the right hemisphere, the cerebellum, hippocampus, striatum, and cerebral cortex tissues were separately dissected and flash frozen on dry ice prior to biochemical analysis as described below.

## Histology

Nissl and Gallyas silver staining were performed on 40 μm free-floating sections using the FD Cresyl Violet™ (cat#PS102-01) and FD NeuroSilver™ Kit II (cat#PK301A) kits from FD NeuroTechnologies according to manufacturer's instructions. For neuron number

studies, the number of Nissl-positive neurons per field was counted by three blinded observers, and the average was determined. Neuronal loss was also determined by a secondary method, NeuN immunohistochemistry (see below), and quantified using Imaris Bitplane automated imaging software. For Layer II/III cortical thickness studies, Nissl stained sections were imaged at 10x magnification using a brightfield microscope. The length between the most superficial point of Layer II and the deepest point of Layer III was measured using Zen Blue microscope and image analysis software. At least 5 measurements were taken per image, 3 images per mouse (n=6 mice/group). For thioflavine S (ThioS) staining, 40 μm sections were mounted onto glass microscope slides and allowed to completely dry. Slides were washed sequentially in 70% and 80% ethanol, 1 min each, prior to incubating in 1% ThioS/80% ethanol solution for 15 min. Sections were then sequentially washed in 80% and 70% ethanol, 1 min each, followed by two rinses in distilled water. Slides were mounted in Prolong Gold antifade reagent and stored in the dark until imaging.

## Immunohistochemistry

For immunohistochemistry (IHC), 40 μm sections prepared as described above were immunostained free-floating in 12-well plates. Sections were washed in Tris buffered saline (TBS), followed by permeabilization in TBS supplemented with 0.05% Triton X-100 (TBS-T), 3 washes 10 min each. Sections were then incubated in citric acid based antigen unmasking solution (Vector Laboratories, cat#H-3300) for 1 h at 70°C. Following antigen retrieval, sections were cooled to room temperature (RT), washed 3 times in TBS-T, and incubated in blocking buffer (TBS-T supplemented with 5% normal donkey serum and 1% bovine serum albumin [BSA]) at RT for 2 h. Sections were then incubated in primary antibody solutions diluted in blocking buffer for 48 h at 4°C. The primary antibodies used were as follows: AT8 (1:100, ThermoFisher Scientific, cat#MN1020), CP13 and PHF1 (1:100, generously provided by P. Davies), TIA1 (1:300, abcam cat#ab40693, lot GR151575-3), PABP (1:300, abcam cat#ab21060), Staufen (1:200, abcam cat#ab73478), DCP1A (1:200, Novus cat#H00055802-MO6), Neurofilament (1:1,000, EMD Millipore cat#AB5539), NeuN (1:1000, EMD Millipore cat#ABN78), and Synaptophysin (1:300, SantaCruz Biotechnology sc-17750). After 48 h, sections were washed 4 times in TBS-T and incubated in donkey Alexa Fluor488/594-conjugated secondary antibodies (Jackson ImmunoResearch) diluted 1:500 in blocking buffer for 2 h at RT. After incubation in secondary antibodies, the sections were washed 2 times in TBS-T, followed by a 20 min incubation in DAPI nuclear stain (1:20,000 in TBS-T), and 2 final washes in TBS-T. Sections were then mounted on microscope slides, immersed in 1% Sudan Black B solution for 15 min to quench endogenous lipofuscin autofluorescence, rinsed 2x in 70% ethanol, and coverslipped using Prolong Gold antifade reagent for imaging using epifluorescence and/or confocal microscopes. All staining steps were performed with gentle agitation. Plates were covered in aluminum foil for all steps following addition of secondary antibodies to prevent photobleaching of fluorophores.

## Biochemical fractionation

Hippocampus and cortex tissues were homogenized in 10x v/w (μL:mg) Hsiao TBS buffer (50 mM Tris, pH 8.0, 274 mM NaCl, 5 mM KCl) supplemented with protease and phosphatase inhibitor cocktails (Roche, cat#05892791001 and cat#04906837001), as

described previously. 100 mg cortical and 50 mg hippocampal homogenates were ultracentrifuged at 28,000 rpm at 4°C for 20 min. The supernatant (S1) fractions were ultracentrifuged a second time at 55,000 rpm at 4°C for 20 min to separate the TBS-extractable supernatant (S1c) and pellet (S1p) fractions. S1p pellets were resuspended in 4x volume of TE buffer relative to the starting weight of the tissue homogenate. Next, the pellet from the first spin (P1) was homogenized in 5x v/w Buffer B (10 mM Tris, pH 7.4, 800 mM NaCl, 10% sucrose, 1 mM EGTA, 1 mM PMSF) using a microcentrifuge pestle, and then ultracentrifuged at 22,000 rpm at 4°C for 30 min. Detergent was then added to the supernatant (S2) fraction to yield a final concentration of 1% sarkosyl, followed by incubation at 37°C on a thermomixer for 1 h. The samples were then ultracentrifuged at 55,000 rpm at 4°C for 1 h to yield the sarkosyl-soluble (S3, supernatant) and sarkosyl-insoluble (P3, pellet) fractions. Finally, RIPA buffer was added to the remaining unused brain homogenates to a final concentration of 50 mM Tris-HCl, 150 mM NaCl, 1% Triton X-100, 0.1% SDS, and 5mM EDTA. S1p, S3, P3, and total (RIPA-soluble) fractions from the same starting tissues were then analyzed by SDS-PAGE as described below. S1p fractions were also shipped to the UMASS Proteomics and Mass Spectrometry facility and analyzed by OrbiTrap liquid-chromatography tandem mass spectrometry, as described previously[13].

## Immunoblot

Reducing and non-reducing protein samples were separated by gel electrophoresis and transferred to nitrocellulose membranes using the Bolt SDS-PAGE system (Life Technologies). Membranes were blocked in 5% nonfat dry milk (NFDM) in TBS supplemented with 0.025% Tween-20 (TBS-T) for 1 h at RT, followed by incubation overnight at 4°C in primary antibody diluted in 5% bovine serum albumin/TBS-T. Primary antibodies used were as follows: Tau5 (1:1000), Tau13 (1:25,000), PHF1 (1:500) and CP13 (1:500) anti-tau antibodies (generously provided by P. Davies); TIA1 (1:500, Santa Cruz Biotechnology, sc-1751), total α-tubulin (1:5000), PABP (1:1000, abcam cat#ab21060), and DDX6 (1:500, Bethyl Labs cat#A300–460A). Membranes were then washed 3 times with TBS-T and incubated in HRP-conjugated secondary antibodies (Jackson ImmunoResearch) diluted in 1% NFDM/TBS-T at RT for 1 h. After incubation in secondary antibody, membranes were washed 3 times in TBS-T and developed using SuperSignal West Pico Chemilluminescent ECL substrate (ThermoFisher Scientific, cat #34080).

## ELISAs

Capture antibodies (Tau5, TNT1, and TOC1) were diluted to a final concentration of 2 ng/μl in phosphate buffered saline (PBS) and adsorbed to Nunc Maxisorp 96-well plates (Cole Palmer, cat#EW-01928-08) for 1 h. Plates were washed 4x in PBS, blocked for 1 h with 5% NFDM/PBS, and washed again 4x in PBS. For non-denaturing analysis of S1 fractions from 9 month PS19 cortex, 20 μg/well samples were diluted in PBS and added to each well in triplicate. Known concentrations of recombinant human tau (WT 0N4R) were used to generate a standard curve. Samples were incubated for 1.5 h at RT, washed 4x in PBS, and then incubated for 1 h with detection antibody (rabbit anti-R1 total tau) diluted 1:10,000 in 5% NFDM/PBS. Plates were washed 4x in PBS followed by incubation with HRP-conjugated donkey anti-rabbit IgG (Jackson ImmunoResearch) diluted 1:5,000 in 5%

NFDM/PBS for 1 h. Plates were washed 4x in PBS and incubated in o-Phenylenediamine (OPD) solution (1 mg/ml OPD in 0.05 sodium phosphate, pH 5.0, 0.05 M citric acid, and 1% hydrogen peroxide) for 15 min at RT. Reactions were stopped using 2.5 M sulfuric acid, and the absorbance was measured at 490 nm.

### Microtubule binding assay

Frozen cortex tissue was homogenized in 10x v/w (μL:mg) RAB buffer (0.1 M MES, pH 6.8, 0.5 mM MgSO4, 1 mM EGTA, 2 mM DTT, 4 M Glycerol, 2 mM GTP, 0.1% Triton X-100). 50 mg homogenate was ultracentrifuged at 50,000 rpm at 30°C for 40 min. Supernantant (S, unbound) fraction was removed to a new microcentrifuge tube and stored at −80°C. Pellet (P, microtubule-bound) fractions were re-suspended in urea buffer (30 mM Tris-HCl, pH 8.4, 8 M urea, 1% CHAPS). 10 μL of each the supernatant and pellet fractions were analyzed by SDS-PAGE.

### Thioflavine T aggregation assay

Recombinant tau and TIA1 were prepared according to standard methods, with purity assessed by coomassie staining after PAGE and by immunoblot. 10 μM recombinant 0N4R tau ± 2 μM recombinant TIA1 was mixed in reaction buffer (10 mM HEPES, 10 mM NaCl, 1 mM DTT, 20 ng/μl RNA, 5 μM thioflavine T) ± 0.04 μg/μl dextran sulfate (DS); negative control samples lacked RNA and DS. Fluorescence was monitored (440 ex/482 em nm) for 48 hrs at 37°C with continual shaking. Tau was phosphorylated with GSK3β (25U/μl; with 1 mM ATP) for 30 min, whereupon the reaction was quenched with 50 mM LiCl.

### Electron microscopy

Mixtures of tau aggregates were prepared using the ThioT aggregation assay described above. 48 h reaction mixtures with or without TIA1 were adsorbed for 2 min onto formvar/carbon-coated Nickel mesh grids, washed 2x with distilled water ($dH_20$), treated with 2% uranyl acetate, washed 4x with $dH_20$ and imaged at 80 kV using a JEOL JEM 1011 with a digital camera (Gatan). For double immuno-gold labeling, grids were rinsed 4x in TBS, blocked for 30 min in block buffer (1% BSA/TBS supplemented with 2.5 μg/ml gelatin, 2% BSAc), and incubated for 2 h in rabbit anti-TIA1 (1:500, Abcam cat#ab40693) and mouse anti-tau (Tau13 or TOC1, 1:1,000) antibodies diluted in block buffer. After 2 h, the grids were washed 4x in TBS prior to incubation for 1 h in 15 nm (anti-rabbit) and 6 nm (anti-mouse) gold particle-conjugated secondary antibodies diluted 1:50 in block buffer. After 1 h, the grids were washed 4x in TBS, then 2x with $dH_2O$ prior to treatment with 2% uranyl acetate. Grids were then washed a final 4x in $dH_2O$ and imaged as described above.

### Image analysis

Images were analyzed for total fluorescence, co-localization, puncta, and cell numbers, as appropriate, using Imaris Bitplane and ImageJ image analysis software. For quantification of stress granules, PABP and TIA1 co-labeled sections were thresholded (TIA1 fluorescence intensity above 69.6, PABP intensity above 9.7) with nuclear masking using DAPI. The number of cytoplasmic (defined by exclusion from DAPI-positive nuclei) puncta with diameter greater than or equal to 2 μm co-positive for both TIA1 and PABP were counted

and divided by the total number of DAPI-positive nuclei per image. For quantification of nuclear versus cytoplasmic immunofluorescence, images were processed as described above, and the total immunofluorescence of TIA1 within (nuclear) and outside (cytoplasmic) of DAPI-positive nuclei was calculated, and divided by the total number of DAPI-positive cells per image. Statistical analysis was performed using GraphPad Prism data analysis software.

### Statistical Analysis

The sample sizes for the experiments were chosen based on prior publications using these mice, which defined the expectations for the effect sizes and variance[16]. The statistical tests performed with data assumptions are described in Supplemental Table S3. Statistical analyses were performed using the GraphPad Prism data analysis software. T-tests were utilized for samples with only two groups. For samples with multiple groups, one and two-way between subjects ANOVA with Tukey's posthoc testing was performed. No data points were excluded. For in vitro experiments (Fig. 7) there are 3–5 replications. For IHC and immunoblotting all experiments include independent samples for replication. Replication was not possible for the behavioral or survival studies.

### Data Availability Statement

All data generated or analyzed during this study are included in this published article (and its supplementary information files). In particular, the proteomics data on the S1p fraction are presented in supplemental table 2.

## Supplementary Material

Refer to Web version on PubMed Central for supplementary material.

## Acknowledgments

We thank Peter Davies (Feinstein Institute) for provision of CP13 and PHF1 antibodies. We would like to thank the following funding agencies for their support: BW: NIH (AG050471, NS089544, ES020395) BrightFocus Foundation, Alzheimer Association, Cure Alzheimer's Fund and the Thome Medical Foundation; UD: UGC-Raman Fellowship, Government of India. TI: NIH (R01 AG054199), HL: Paul F. Glenn Foundation.

## References

1. Gitler AD, Shorter J. RNA-binding proteins with prion-like domains in ALS and FTLD-U. Prion. 2011; 5:179–187. [PubMed: 21847013]
2. Ash PE, Vanderweyde TE, Youmans KL, Apicco DJ, Wolozin B. Pathological stress granules in Alzheimer's disease. Brain Res. 2014; 1584:52–58. [PubMed: 25108040]
3. Banani SF, Lee HO, Hyman AA, Rosen MK. Biomolecular condensates: organizers of cellular biochemistry. Nat Rev Mol Cell Biol. 2017; 18:285–298. [PubMed: 28225081]
4. Feric M, et al. Coexisting Liquid Phases Underlie Nucleolar Subcompartments. Cell. 2016; 165:1686–1697. [PubMed: 27212236]
5. Anderson P, Kedersha N. Stress granules: the Tao of RNA triage. Trends Biochem Sci. 2008; 33:141–150. [PubMed: 18291657]
6. Panas MD, Ivanov P, Anderson P. Mechanistic insights into mammalian stress granule dynamics. J Cell Biol. 2016; 215:313–323. [PubMed: 27821493]
7. Irwin DJ, et al. Frontotemporal lobar degeneration: defining phenotypic diversity through personalized medicine. Acta Neuropathol. 2015; 129:469–491. [PubMed: 25549971]

8. Jain A, Vale RD. RNA phase transitions in repeat expansion disorders. Nature. 2017; 546:243–247. [PubMed: 28562589]
9. Patel A, et al. A Liquid-to-Solid Phase Transition of the ALS Protein FUS Accelerated by Disease Mutation. Cell. 2015; 162:1066–1077. [PubMed: 26317470]
10. Nott TJ, et al. Phase transition of a disordered nuage protein generates environmentally responsive membraneless organelles. Mol Cell. 2015; 57:936–947. [PubMed: 25747659]
11. Molliex A, et al. Phase Separation by Low Complexity Domains Promotes Stress Granule Assembly and Drives Pathological Fibrillization. Cell. 2015; 163:123–133. [PubMed: 26406374]
12. Lin Y, Protter DS, Rosen MK, Parker R. Formation and Maturation of Phase-Separated Liquid Droplets by RNA-Binding Proteins. Mol Cell. 2015; 60:208–219. [PubMed: 26412307]
13. Vanderweyde T, et al. Interaction of tau with the RNA-binding Protein TIA1 Regulates tau Pathophysiology and Toxicity. Cell reports. 2016; 15:1–12. [PubMed: 27052168]
14. Vanderweyde T, et al. Contrasting Pathology of Stress Granule Proteins TIA-1 and G3BP in Tauopathies. J Neurosci. 2012; 32:8270–8283. [PubMed: 22699908]
15. Wang Y, Mandelkow E. Tau in physiology and pathology. Nat Rev Neurosci. 2016; 17:5–21. [PubMed: 26631930]
16. Yoshiyama Y, et al. Synapse loss and microglial activation precede tangles in a P301S tauopathy mouse model. Neuron. 2007; 53:337–351. [PubMed: 17270732]
17. Phillips K, Kedersha N, Shen L, Blackshear PJ, Anderson P. Arthritis suppressor genes TIA-1 and TTP dampen the expression of tumor necrosis factor alpha, cyclooxygenase 2, and inflammatory arthritis. Proc Natl Acad Sci U S A. 2004; 101:2011–2016. [PubMed: 14769925]
18. Takeuchi H, et al. P301S mutant human tau transgenic mice manifest early symptoms of human tauopathies with dementia and altered sensorimotor gating. PLoS One. 2011; 6:e21050. [PubMed: 21698260]
19. Lalonde R. The neurobiological basis of spontaneous alternation. Neurosci Biobehav Rev. 2002; 26:91–104. [PubMed: 11835987]
20. Cohen SJ, Stackman RW Jr. Assessing rodent hippocampal involvement in the novel object recognition task. A review. Behav Brain Res. 2015; 285:105–117. [PubMed: 25169255]
21. Abraha A, et al. C-terminal inhibition of tau assembly in vitro and in Alzheimer's disease. J Cell Sci. 2000; 113(Pt 21):3737–3745. [PubMed: 11034902]
22. Ding H, Matthews TA, Johnson GV. Site-specific phosphorylation and caspase cleavage differentially impact tau-microtubule interactions and tau aggregation. J Biol Chem. 2006; 281:19107–19114. [PubMed: 16687396]
23. Rocher AB, et al. Structural and functional changes in tau mutant mice neurons are not linked to the presence of NFTs. Exp Neurol. 2010; 223:385–393. [PubMed: 19665462]
24. Santacruz K, et al. Tau suppression in a neurodegenerative mouse model improves memory function. Science. 2005; 309:476–481. [PubMed: 16020737]
25. de Calignon A, et al. Caspase activation precedes and leads to tangles. Nature. 2010; 464:1201–1204. [PubMed: 20357768]
26. Sanders DW, et al. Distinct tau prion strains propagate in cells and mice and define different tauopathies. Neuron. 2014; 82:1271–1288. [PubMed: 24857020]
27. Kuchibhotla KV, et al. Neurofibrillary tangle-bearing neurons are functionally integrated in cortical circuits in vivo. Proc Natl Acad Sci U S A. 2014; 111:510–514. [PubMed: 24368848]
28. Sahara N, et al. Characteristics of TBS-extractable hyperphosphorylated tau species: aggregation intermediates in rTg4510 mouse brain. J Alzheimers Dis. 2013; 33:249–263. [PubMed: 22941973]
29. Berger Z, et al. Accumulation of pathological tau species and memory loss in a conditional model of tauopathy. J Neurosci. 2007; 27:3650–3662. [PubMed: 17409229]
30. Combs B, Hamel C, Kanaan NM. Pathological conformations involving the amino terminus of tau occur early in Alzheimer's disease and are differentially detected by monoclonal antibodies. Neurobiol Dis. 2016; 94:18–31. [PubMed: 27260838]
31. Huang da W, Sherman BT, Lempicki RA. Systematic and integrative analysis of large gene lists using DAVID bioinformatics resources. Nat Protoc. 2009; 4:44–57. [PubMed: 19131956]

32. Li YR, King OD, Shorter J, Gitler AD. Stress granules as crucibles of ALS pathogenesis. J Cell Biol. 2013; 201:361–372. [PubMed: 23629963]
33. Wolozin B. Regulated protein aggregation: stress granules and neurodegeneration. Mol Neurodegener. 2012; 7:56. [PubMed: 23164372]
34. Dobson CM. Protein folding and misfolding. Nature. 2003; 426:884–890. [PubMed: 14685248]
35. Li P, et al. Phase transitions in the assembly of multivalent signalling proteins. Nature. 2012; 483:336–340. [PubMed: 22398450]
36. Maziuk B, Ballance HI, Wolozin B. Dysregulation of RNA Binding Protein Aggregation in Neurodegenerative Disorders. Frontiers in molecular neuroscience. 2017; 10
37. Taylor JP, Brown RH Jr, Cleveland DW. Decoding ALS: from genes to mechanism. Nature. 2016; 539:197–206. [PubMed: 27830784]
38. Banani SF, et al. Compositional Control of Phase-Separated Cellular Bodies. Cell. 2016; 166:651–663. [PubMed: 27374333]
39. Brunello CA, Yan X, Huttunen HJ. Internalized Tau sensitizes cells to stress by promoting formation and stability of stress granules. Sci Rep. 2016; 6:30498. [PubMed: 27460788]
40. Meier S, et al. Pathological Tau Promotes Neuronal Damage by Impairing Ribosomal Function and Decreasing Protein Synthesis. J Neurosci. 2016; 36:1001–1007. [PubMed: 26791227]
41. Zhang X, et al. RNA stores tau reversibly in complex coacervates. PLoS Biol. 2017; 15:e2002183. [PubMed: 28683104]
42. Zempel H, Mandelkow E. Lost after translation: missorting of Tau protein and consequences for Alzheimer disease. Trends Neurosci. 2014; 37:721–732. [PubMed: 25223701]
43. Ling SC, Polymenidou M, Cleveland DW. Converging mechanisms in ALS and FTD: disrupted RNA and protein homeostasis. Neuron. 2013; 79:416–438. [PubMed: 23931993]
44. Darnell RB. RNA protein interaction in neurons. Annu Rev Neurosci. 2013; 36:243–270. [PubMed: 23701460]
45. Leger M, et al. Object recognition test in mice. Nat Protoc. 2013; 8:2531–2537. [PubMed: 24263092]

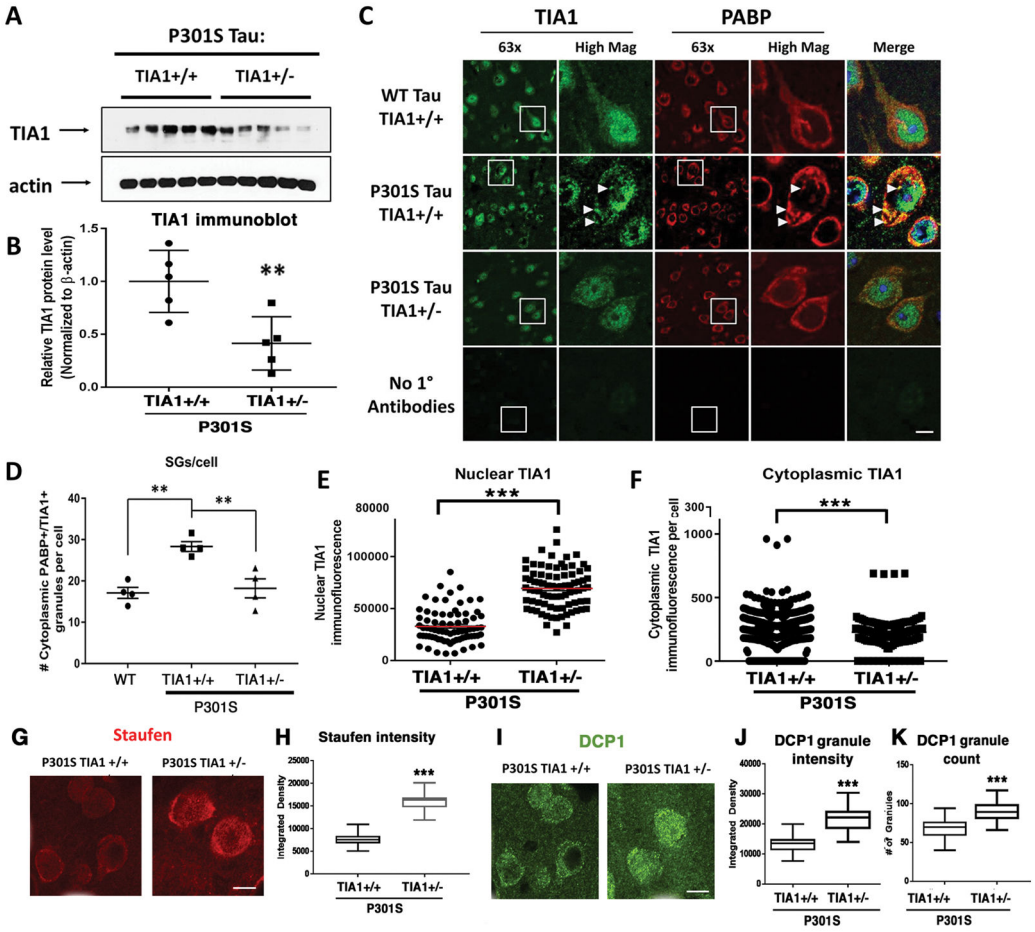


**Figure 1. TIA1 reduction decreases cytoplasmic stress granules in PS19 mice while increasing nuclear TIA1**

A. Immunoblot of TIA1 from total brain lysates of 3 month old P301S *Tia1+/+* and P301S *Tia1+/−* mice. **B.** Quantification of relative TIA1 protein level normalized to β-actin from A. **p=0.0095 by unpaired Student's t-test (n=5/group). **C.** IHC of DAPI (blue), TIA1 (green), and PABP (red) in 9 month Layer II LEnt. Scale bar = 5 μm. **D.** Quantification of the number of cytoplasmic puncta per cell co-positive for the SG markers TIA1 and PABP (arrows) from C. **P<0.01 by 1-way ANOVA with Tukey's post-hoc tests (n=4 mice/group, at least 20 cells imaged per mouse). **E–F.** Quantification of total nuclear (E) and cytoplasmic (F) TIA1 immunofluorescence from C. ***p<0.001 by unpaired Student's t-test. **G–H.** IHC of the RNA transport granule marker Staufen (G, red) and the P-body marker DCP1A (H, green) in 9 month P301S *Tia1+/+* and P301S *Tia1+/−* frontal cortex. Scale bar = 10 μm. **I–K.** Quantification of total Staufen immunofluorescence (I), total DCP1A immunofluorescence (J), and number of cytoplasmic DCP1A granules (K) per cell in G and H. ***P<0.001 by unpaired Student's t-test (n=4 mice/group, at least 20 cells imaged per mouse). Error bars represent means ± SEM. The immunoblots in panel 1A are cropped; full gel pictures for all immunoblots are shown in Supplemental Figures 16–21.

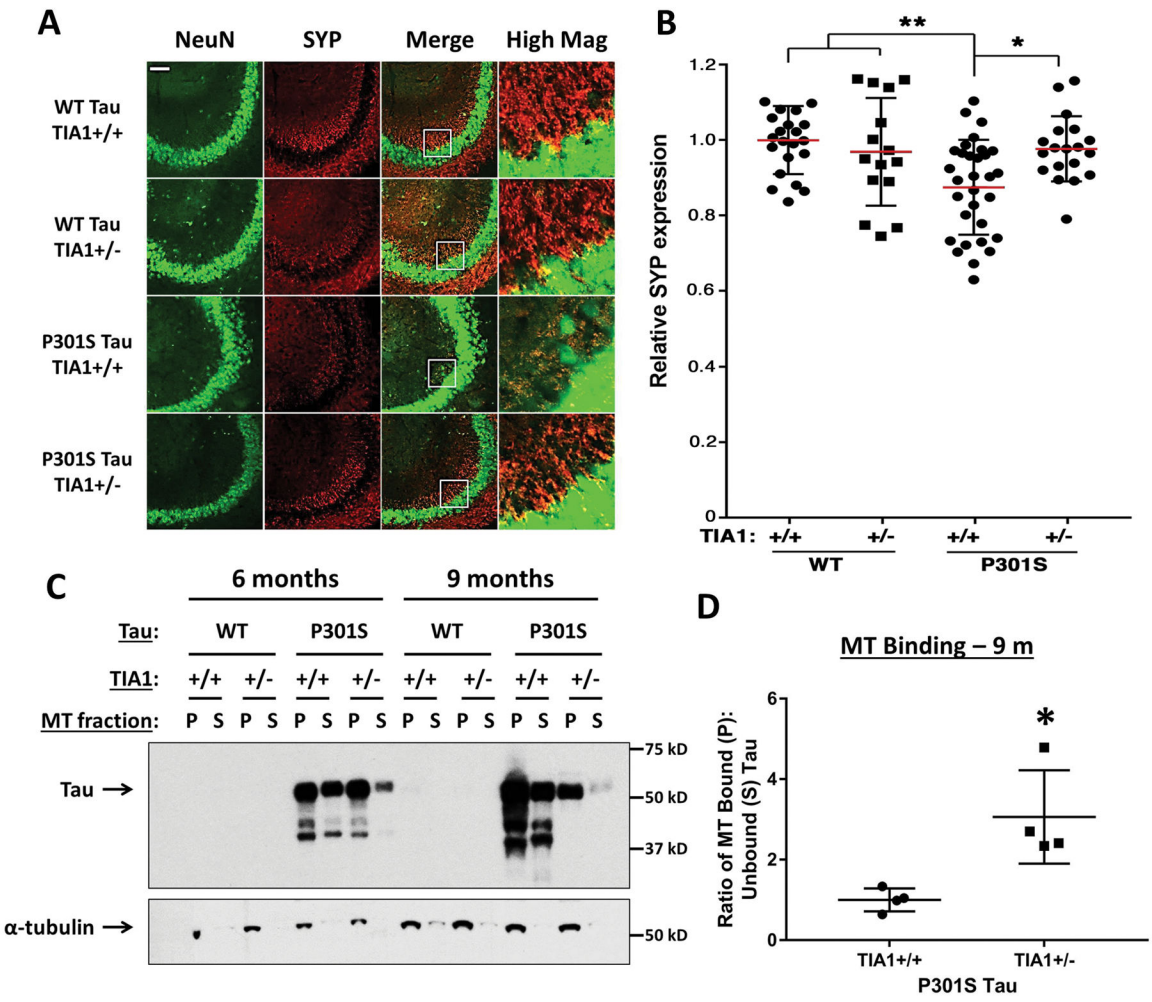


**Figure 2. TIA1 reduction rescues synaptic and axonal loss in PS19 mice**

**A.** IHC of NeuN (green) and synaptophysin (SYP, red) in the CA3 region of 6 month non-transgenic (WT Tau) and PS19 (P301S Tau) hippocampus. Scale bar = 20 μm. **B.** Quantification of relative SYP expression from A. *P=0.0135 **P=0.0067 by 2-way ANOVA with Tukey's post-hoc test (n=15–31 images/group, from at least 6 mice/group). **C.** Immunoblot of total tau (Tau13) detected in microtubule (MT)-bound (pellet, P) and unbound (supernatant, S) fractions in 6 and 9 month WT and PS19 cortex. **D.** Quantification of the relative ratio of MT-bound to MT-unbound tau at 9 months in A (normalized to the average level in P301S *Tia1+/+* mice equal to 1). *p=0.0138 by Student's t-test (n=4/group). Error bars denote means ± SEM. The immunoblots in panel 2C are cropped.

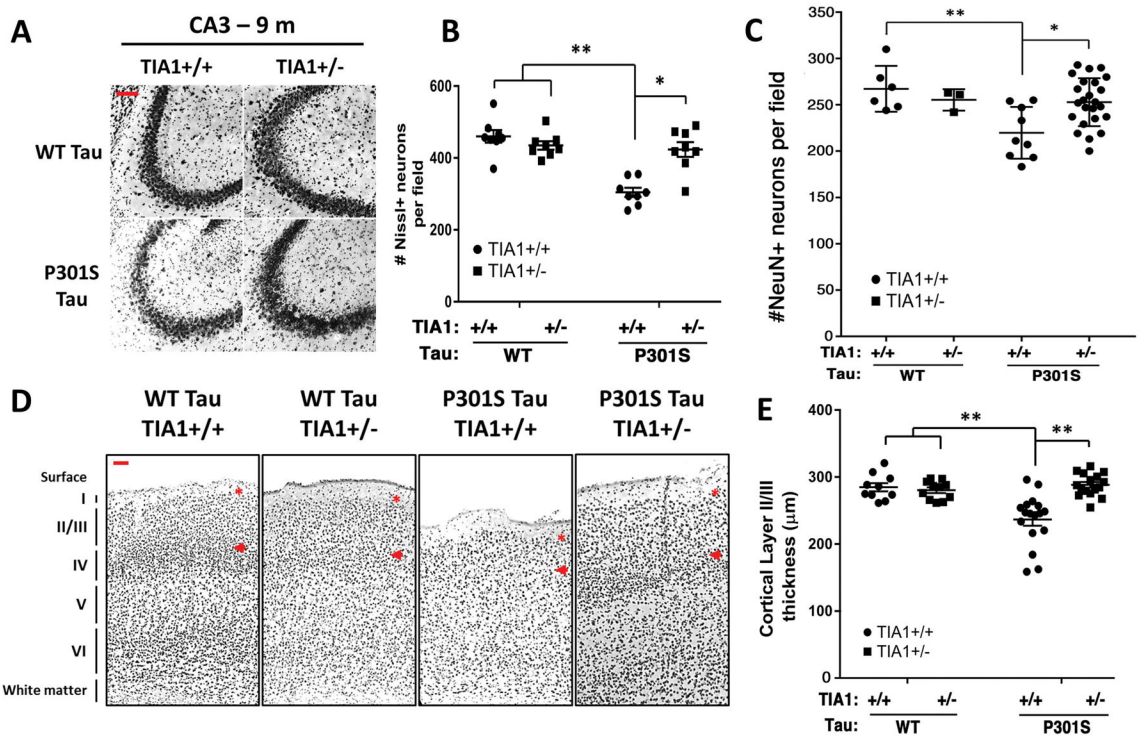


**Figure 3. TIA1 reduction protects against neurodegeneration in PS19 mice**

**A.** Representative Nissl stain of CA3 in 9 month (m) non-transgenic (WT tau) and PS19 (P301S tau) mice. Scale bar = 20 μm. **B–C.** Quantification of number of Nissl+ (B) and NeuN+ (C) neurons per field in C. *P<0.05 **P<0.01 by 2-way ANOVA with Tukey's post-hoc tests (n=at least 4/group). **D.** Representative images of cortical layers I through VI in 9 month non-transgenic and PS19 cerebral cortex (primary somatosensory cortex, S1). Scale bar = 100 μm. Red asterisks and arrowheads denote the start of Layer II and end of Layer III, respectively. **E.** Quantification of average Layer II/III cortical thickness in S1 from D. **P<0.01 by 2-way ANOVA with Tukey's post-hoc tests (n=at least 11/group). Error bars denote means ± SEM.

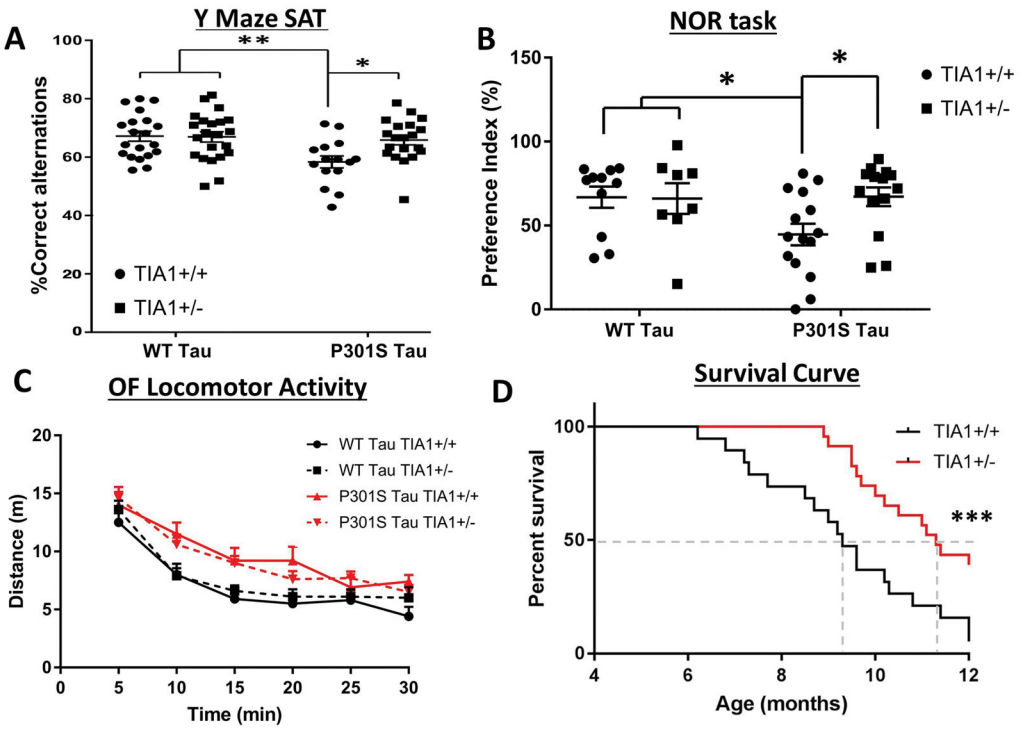


**Figure 4. TIA1 reduction improves memory and prolongs lifespan in PS19 mice**

**A.** Percent correct alternations in the Y maze spontaneous alternation task (SAT) for 6 month non-transgenic (WT Tau) and PS19 (P301S Tau) mice. *P=0.0213 **P=0.0072 by 2-way ANOVA with Tukey's post-hoc test (n=16–20 mice/group). Error bars denote means ± SEM. **B.** The novel object recognition (NOR) task was used to assess recognition memory in non-transgenic and PS19 mice. Preference index (PI) for each mouse was determined by dividing the amount of time spent exploring the novel object by the total amount of time spent exploring both objects (PI = 100 * ($T_{novel}$/$T_{novel}$ + $T_{familiar}$). *p<0.05 by 2-Way ANOVA with Tukey's post-hoc comparisons (n=8–15 mice/group). Error bars denote means ± SEM. **C.** Total distance traveled over time in the Open Field (OF) locomotor activity task. Main effect of P301S tau transgene (***P<0.001) by 2-way ANOVA; P301S *Tia1+/+* and P301S *Tia1+/−* plots are not statistically different by Tukey's post-hoc test. **D.** Kaplan-Meier survival curve of P301S *Tia1+/+* (n=20, median lifespan=9.3 months) compared to P301S *Tia1+/−* (n=23, median lifespan=11.3 months) mice. ***P<0.001 by the Log-rank Mantel-Cox test. Hazard ratio (*Tia1+/+:Tia1+/−*) = 2.411.

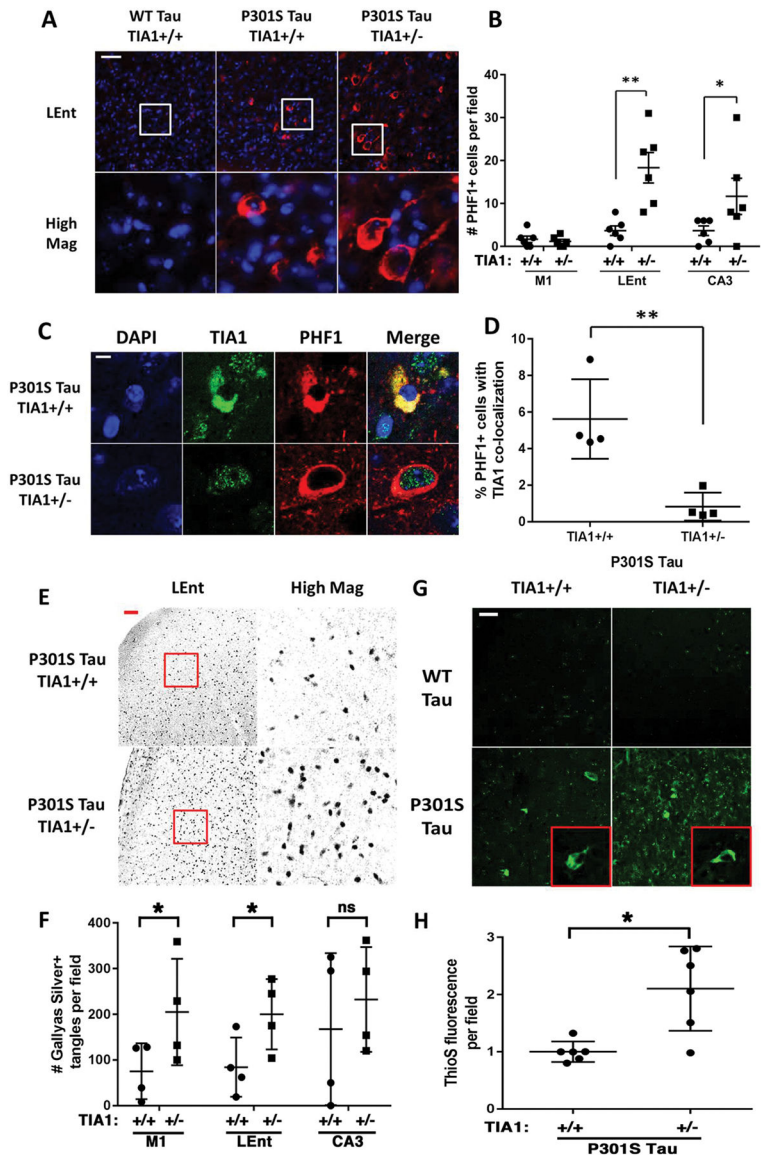


**Figure 5. TIA1 reduction leads to an age-dependent increase in tau phosphorylation**

**A.** IHC of DAPI (blue) and PHF1 (S396/S404) phospho-tau in the lateral entorhinal cortex (LEnt) of 9 month old P301S *Tia1+/+* and P301S *Tia1+/−* mice. Scale bar = 10 μm. **B.** Quantification of number of PHF1+ cells in D. *P=0.0483 **P=0.0028 by unpaired Student's T-tests (n=6/group). **C.** Confocal images of PHF1+ cells in P301S *Tia1+/+* and P301S *Tia1+/−* LEnt. Scale bar = 2 μm. **D.** Quantification of the percentage of PHF1+ cells with TIA1 co-localization in F. **P=0.0074 by Student's t-test (n=4/group). **E.** Representative images of Gallyas Silver stained neurofibrillary tangles in 9 month P301S *Tia1+/+* and P301S *Tia1+/−* mice. Scale bar = 40 μm. **F.** Quantification of number of Gallyas Silver+ tangles in the frontal cortex (primary motor area, M1), lateral entorhinal cortex (LEnt), and CA3. *P<0.05 by unpaired Student's T-tests (n=4/group). **G.** Representative images of LEnt from 9 month non-transgenic and PS19 mice stained with thioflavine S (ThioS). Scale bar = 20 μm. Red inserts denote high magnification images of

ThioS+ tangles in P301S *Tia1+/+* and P301S *Tia1+/−* LEnt. **H.** Quantification of ThioS fluorescence in G. *P=0.0213 by Student's t-test (n=6/group). Error bars denote means ± SEM.

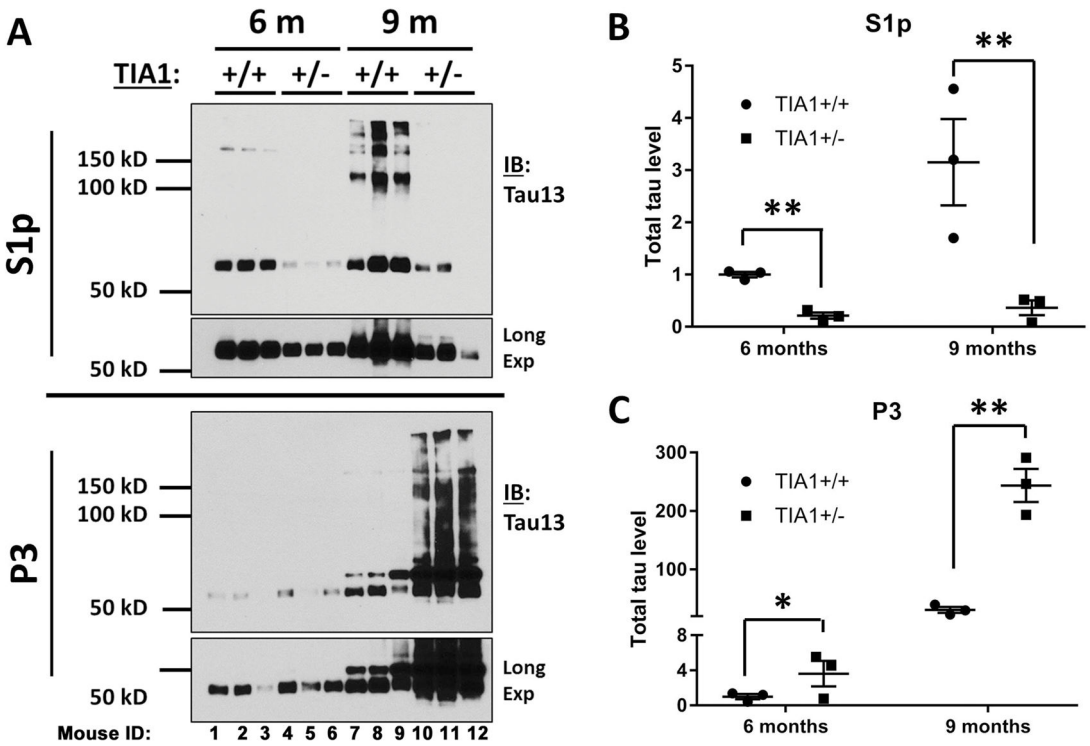


**Figure 6. TIA1 reduction shifts the biochemical and structural properties of tau aggregation**

**A.** Immunoblot for total tau (Tau13) in the S1p (top) and P3 (bottom) fractions of 6 and 9 month P301S *Tia1+/+* and P301S *Tia1+/−* cortex. Each lane corresponds to a different mouse from the cohort. **B–C.** Quantification of tau accumulation in the S1p (B) and P3 (C) fractions in A. #p=0.1508 *p=0.0289 **p=0.0018 ***p=0.0005 by unpaired Student's T-tests (n=3/group). Error bars denote mean ± SEM. The immunoblots in panel 6A are cropped.

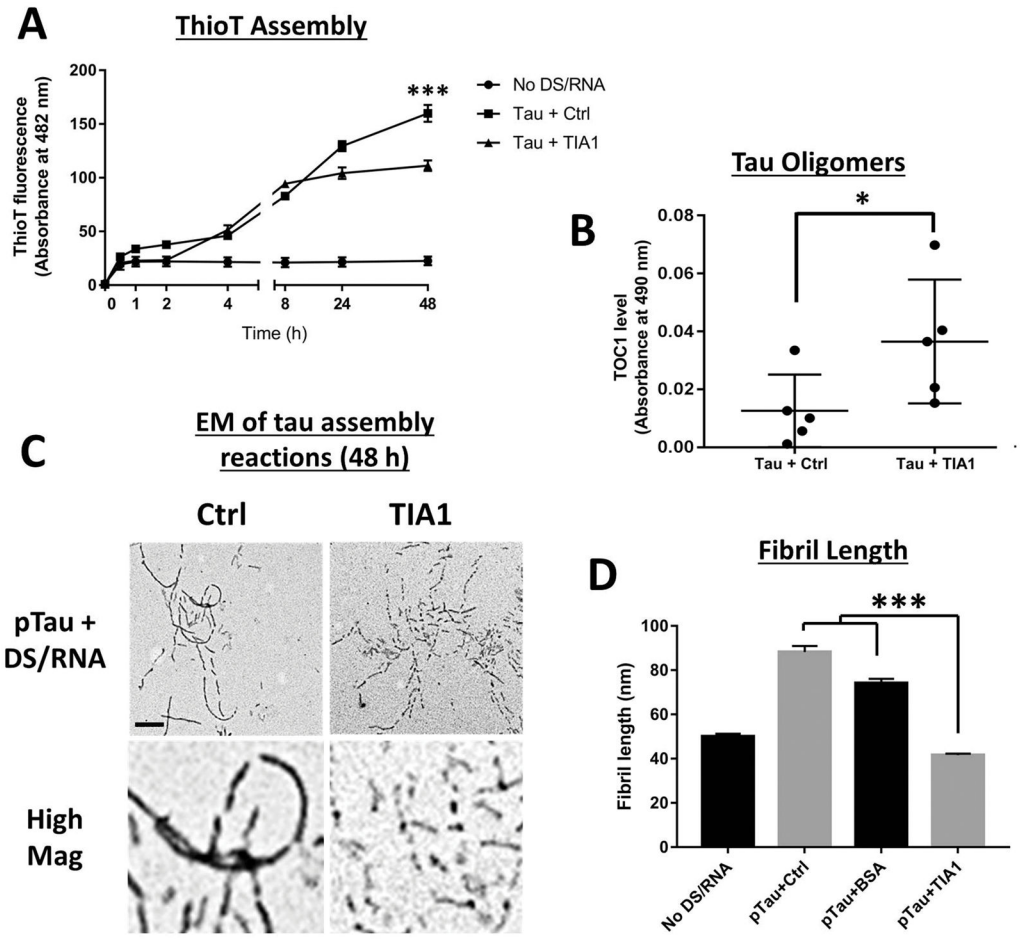


**Figure 7. TIA1 inhibits tau fibrillization while increasing tau oligomerization**

**A.** Thioflavine T (ThioT) fluorescence assay of GSK3β-phosphorylated recombinant tau protein (pTau, 10 μM) incubated with dextran sulfate (DS, 0.04 μg/μl) and RNA (20 ng/μl) go induce aggregation ± recombinant TIA1 protein (2 μM). The presence of TIA1 in the reaction mixture significantly reduced the amount of ThioT fluorescence. ***P<0.001 by repeated measures 2-Way ANOVA with Tukey's post-hoc comparisons (n=4/group). **B.** TOC1 level detected by ELISA in ThioT reaction mixtures after 48 h in the absence (Tau + Ctrl) and presence of TIA1 (Tau + TIA1). 2 μM bovine serum albumin (BSA) was used as a control. *P<0.05 by unpaired Student's t-test (n=5/group). **C.** Representative transmission electron microscopy (EM) of pTau assembly reactions incubated ± TIA1. Scale Bar = 500 nm. Bottom panels represent high magnification images to visualize fibril length and structure. **D.** Quantification of fibril lengths from C. ***P<0.001 by 1-Way ANOVA with Tukey's post-hoc comparisons (n=4/group; at least 100 fibrils measured per condition). Error bars denote means ± SEM. Experiments in this figure have been replicated three times.